

Partitioned Algorithms using Vortex Particle Methods for Fluid–Structure Interaction of Thin-walled Flexible Structures

DISSERTATION

zur Erlangung des akademischen Grades
Doktor-Ingenieur (Dr.-Ing.)

an der Fakultät Bauingenieurwesen
der Bauhaus-Universität Weimar

vorgelegt von

Samir Chawdhury

geboren am 03 Juni 1984
in Netrokona, Bangladesch

Gutachter: Prof. Dr. Guido Morgenthal
Prof. Dr. Kincho Law
Prof. Dr.-Ing. Matthias Kraus

Weimar, 24. März 2021

*To
my mother Hena
my wife Sharmistha
my daughter Aishani and my son Ishaan*

EHRENWÖRTLICHE ERKLÄRUNG

Ich erkläre hiermit ehrenwörtlich, dass ich die vorliegende Arbeit ohne unzulässige Hilfe Dritter und ohne Benutzung anderer als der angegebenen Hilfsmittel angefertigt habe. Die aus anderen Quellen direkt oder indirekt übernommenen Daten und Konzepte sind unter Angabe der Quelle gekennzeichnet.

Bei der Auswahl und Auswertung folgenden Materials haben mir die nachstehend aufgeführten Personen in der jeweils beschriebenen Weise entgeltlich/unentgeltlich geholfen:

Keine.

Weitere Personen waren an der inhaltlich-materiellen Erstellung der vorliegenden Arbeit nicht beteiligt. Insbesondere habe ich hierfür nicht die entgeltliche Hilfe von Vermittlungs- bzw. Beratungsdiensten (Promotionsberater oder anderer Personen) in Anspruch genommen. Niemand hat von mir unmittelbar oder mittelbar geldwerte Leistungen für Arbeiten erhalten, die im Zusammenhang mit dem Inhalt der vorgelegten Dissertation stehen.

Die Arbeit wurde bisher weder im In- noch im Ausland in gleicher oder ähnlicher Form einer anderen Prüfungsbehörde vorgelegt.

Ich versichere ehrenwörtlich, dass ich nach bestem Wissen die reine Wahrheit gesagt und nichts verschwiegen habe.

Weimar, den 24.03.2021

Signature

.....

Samir Chawdhury

Acknowledgements

First and foremost, I am extremely grateful to my supervisor, Professor Guido Morgenthal, for his precious guidance, endless support, and patience throughout my PhD study. His immense knowledge and ample experience have encouraged me in my academic research. I have learned a lot, particularly from his thought process when dealing with a research problem and handling it in small and simple steps. His thoughtful comments, practical criticism and appreciation helped me a lot to achieve my research outcome.

I would also like to thank Professor Kincho Law and Professor Matthias Kraus for reviewing my dissertation and providing constructive comments. My special thanks go to Professor Law and his research group for their wind tunnel experiment results, which served as the foundation of my research. I would like to thank Professor Klaus Gürlebeck for his teaching and cooperation during my studies at Bauhaus University Weimar.

I would like to appreciate my colleague Dr.-Ing. Khaled Ibrahim Tolba a lot for teaching me about computational programming and dealing with technical problems. I would also like to thank Benjamin Bendig for his technical support. My unlimited thanks go to another colleague Dr.-Ing. Tajammal Abbas. I find myself lucky to share my office room with a person like him for so many years. Many thanks go for his support from an academic and personal point of view.

I am lucky to work with a lot of friendly and supportive colleagues in MSK. I would like to thank Dr.-Ing. Amir Hossein Arshain and Dr.-Ing. Dario Milani, Victor Vilceanu, and Dr.-Ing. Igor Kavrakov not only for sharing the office with me but also for being so friendly. I would like to thank also my colleague Sebastian Rau for helping me unconditionally. Thanks to my colleagues Dr.-Ing. Hans-Georg Timmler, Dr.-Ing. Wei Wang, Christopher Taube, Normann Hallermann, Marcel Helmrich, Jakob Taraben, Anne-Marie Nöthlich and Jutta Lorenz for making this time so memorable.

I would like to express my gratitude to Bauhaus Research school and the German Research Foundation (DFG) for financing my research.

I wouldn't be here without the continuous support and prayers of my parents. It is beyond my words to describe my gratitude, especially to my mother, Hena Chowdhury, a selfless and soulful person. I also like to express my thanks to my lovely sisters Suborna and Suma and my brother-in-law Sajib for their support.

I can't imagine my life without the unending support and love of my wife and my best friend Sharmistha Chowdhury. She has always been my inspiration. It has been an incredible journey with her since 2004 when we were studying together for our Bachelor degree. Thanks to God to fulfil our family with two wonderful children, Aishani and Ishaan. I also like to thank my sister-in-law Shaswati for her inspiration. My special thanks go to my mother-in-law Krishna Chowdhury for her encouragement, support and blessings.

Samir Chawdhury
Weimar, 2021

Abstract

Fluid–structure interaction (FSI) is a multiphysics study of mutual interaction between deformable structure and surrounding or internal fluid flow. Proper understanding of FSI phenomena is crucial in many engineering fields. The increasing trend of extremely flexible and lightweight structures, such as long-span cable-supported bridges, super-tall towers and chimneys, large membrane roofs, requires accurate prediction of wind–structure interaction in the design process to avoid potential damage of important structures.

The grid-free Vortex Particle Method (VPM) has been established as an accurate and efficient computational fluid dynamic (CFD) simulation technique to model flow around complex geometries. Existing FSI models of VPM have been in the context of two-dimensional (2D) and pseudo-three-dimensional (pseudo-3D) multi-slice formulations. They are based on linear structural behaviour and limited to rigid cross-sections only. In this study, the VPM is extended with new developments to enhance its applicability for coupled FSI simulations of thin-walled flexible structures. The partitioned algorithms are employed to implement the coupling of flow solvers, 2D and pseudo-3D VPM, with advanced structural models.

Initially, the 2D VPM is coupled with corotational finite element formulation, which is to include geometric nonlinear effects for large-displacement FSI of thin plate systems. Fundamentally, at each simulation step, the fluid forces are projected from the surface panels to the FE nodes at the mid-surface of the thin body. The nodal displacements are projected as feedback to the surface panels to update the required boundary conditions. The coupled solver is validated on benchmark large-displacement FSI problems such as the flag-type flapping of cantilever plates in axial flow and Kármán vortex street. The validated extension of 2D VPM is successfully employed for analysing diverse and complex aeroelastic interactions of different thin-walled systems such as a) inverted and T-shaped cantilevers with/without tip mass, b) flexible membrane systems, and c) umbrella-type structures.

Secondly, the pseudo-3D VPM is extended similarly according to the procedure of 2D VPM, however, in a slice-wise manner. Importantly, the pseudo-3D VPM is proposed for FSI analysis of linear shell structures. Modal superposition technique is applied because of its computational efficiency. The novelty is the inclusion of 3D natural vibration modes in the structural analysis. The validated method is utilised for the aeroelastic interaction of shell-type structures such as large membrane roof and solar chimneys.

Furthermore, two new extensions of 2D VPM are developed for modelling of inflow fluctuations that can be used as inflow condition in FSI analysis. While the first extension allows modelling of low-frequency pulsating incoming flow, the second extension reproduces turbulent wakes from bluff bodies. Finally, the FSI model of 2D VPM is applied exclusively to a distinct application field: small-scale aeroelastic energy harvesting. The aero-electromechanically coupled behaviour is modelled for different thin and flexible prototype harvesters. An analysis framework is shown useful for optimisation of harvester performance for different inflow conditions. This work indicates that the developed numerical techniques are beneficial not only for fundamental investigations but also for aeroelastic interaction of large-scale thin-walled mega structures.

Kurzfassung

Die Fluid–Struktur-Kopplung, FSK (oder FSI im internationalen Kontext) ist ein multiphysikalischer Effekt der gegenseitigen Wechselwirkung zwischen verformbarer Struktur und umgebender oder interner Fluidströmung. Das richtige Verständnis der FSI-Phänomene ist in vielen technischen Bereichen von entscheidender Bedeutung. Der zunehmende Trend zu extrem flexiblen und leichten Strukturen, wie z.B. weitgespannte seilunterstützte Brücken, superhohe Türme und Schornsteine, große Membrandächer, erfordert eine genaue Vorhersage der Wind–Struktur-Kopplung (WSK) im Entwurfsprozess, um potenzielle Schäden an wichtigen Strukturen zu vermeiden.

Die gitterfreie Vortex-Partikel-Methode (VPM) wurde als genaue und effiziente numerischen Strömungsmechanik (CFD im internationalen Kontext) Simulationstechnik zur Modellierung der Strömung um komplexe Geometrien herum etabliert. Bestehende FSI-Modelle der VPM wurden im Zusammenhang mit zweidimensionalen (2D) und pseudodreidimensionalen (Pseudo-3D) Mehrschichtformulierungen erstellt. Sie basieren auf linearem Strukturverhalten und sind nur auf starre Querschnitte beschränkt. In dieser Studie wird das VPM um neue Entwicklungen erweitert, um seine Anwendbarkeit für gekoppelte FSI-Simulationen von dünnwandigen flexiblen Strukturen zu verbessern. Die partitionierten Algorithmen werden eingesetzt, um die Kopplung von Strömungslösern, 2D und Pseudo-3D VPM, mit fortschrittlichen Strukturmodellen zu implementieren.

Zunächst wird der 2D VPM mit einer korotationalen Finite-Elemente-Formulierung gekoppelt, die geometrisch nichtlineare Effekte für FSI mit großer Verschiebung von dünnen Plattensystemen beinhalten soll. Grundsätzlich werden bei jedem Simulationsschritt die Fluidkräfte von den Oberflächenplatten auf die FE-Knoten in der Mittelfläche des dünnen Körpers projiziert. Die Knotenverschiebungen werden als Rückkopplung auf die Oberflächenplatten projiziert, um die erforderlichen Randbedingungen zu aktualisieren. Der gekoppelte Solver wird anhand von FSK-Benchmark-Problemen mit großen Verschiebungen validiert, wie z.B. das fahnenartige Flattern von Cantilever-Platten in axialer Strömung und Kármán Wirbelstraße. Die validierte Erweiterung von 2D VPM wird erfolgreich zur Analyse vielfältiger und komplexer aeroelastischer Wechselwirkungen verschiedener dünnwandiger Systeme eingesetzt, wie z.B. a) invertierte und T-förmige Cantilever mit/ohne Spitzenmasse, b) flexible Membransysteme und c) schirmartige Strukturen.

Zweitens wird die Pseudo-3D-VPM nach dem Verfahren der 2D-VPM in ähnlicher Weise erweitert, jedoch scheibenweise. Wichtig ist, dass die Pseudo-3D VPM für die FSI-Analyse von linearen Schalenstrukturen vorgeschlagen wird. Die modale Überlagerungstechnik wird wegen ihrer rechnerischen Effizienz angewendet. Das Novum ist die Einbeziehung von 3D-Eigenschwingungsmoden in die Strukturanalyse. Die validierte Methode wird für die aeroelastische Wechselwirkung von schalenartigen Strukturen wie großen Membrandächern und Solarkaminen eingesetzt.

Darüber hinaus werden zwei neue Erweiterungen von 2D VPM zur Modellierung von Einströmschwankungen entwickelt, die als Einströmbedingung in der FSK-Analyse verwendet werden können. Während die erste Erweiterung die Modellierung von niederfrequent pulsierender Einströmung ermöglicht, reproduziert die zweite Erweiterung turbulente Nachläufe von Steilkörpern. Schließlich wird das FSI-Modell der 2D-VPM ausschließlich auf ein bestimmtes Anwendungsgebiet angewandt: die kleinräumige aeroelastische Energiegewinnung. Das aero-elektro-mechanisch gekoppelte Verhalten wird für verschiedene dünne und flexible

Prototyp-Harvester modelliert. Es wird ein Analyserahmen gezeigt, der für die Optimierung der Harvesterleistung für verschiedene Einströmbedingungen nützlich ist. Diese Arbeit zeigt, dass die entwickelten numerischen Techniken nicht nur für grundlegende Untersuchungen, sondern auch für die aeroelastische Wechselwirkung großflächiger dünnwandiger Megastrukturen von Nutzen sind.

Contents

Acknowledgements	VII
Abstract	IX
Table of Contents	XIII
List of figures	XVII
List of tables	XXV
Nomenclature	XXVII
1 Introduction	1
1.1 Background and motivation	1
1.2 Objectives, methodologies and contributions	3
1.3 Outline of the thesis	5
2 Wind effects on structures	7
2.1 Introduction	7
2.2 Atmospheric boundary layer	7
2.3 Bluff body aerodynamics	9
2.4 Aeroelastic vibration phenomena	10
2.4.1 Limited amplitudes phenomena	11
2.4.2 Divergent amplitudes phenomena	12
2.5 Nonlinear aeroelasticity	13
2.6 Summary	14
3 Numerical methods for fluid–structure interaction simulation	15
3.1 Introduction	15
3.2 Coupling mechanisms for FSI simulations	16
3.2.1 Monolithic approaches	16
3.2.2 Partitioned approaches	17
3.2.3 Conforming and non-conforming mesh	18
3.2.4 Large displacement FSI simulations	18
3.3 Numerical analysis of fluid and structure	19
3.3.1 Modelling of fluid motion	19
3.3.2 Structural analysis using finite element methods	20
3.4 The Vortex Particle Method	20
3.4.1 Governing equations of fluid motion	21
3.4.2 The Boundary Element Method	23
3.5 Application of Vortex methods	25

3.5.1	Aerodynamic analysis of bluff bodies	25
3.5.2	Studies of deformable bodies using vortex methods	27
3.6	Summary	28
4	Partitioned extensions using Vortex Particle Methods for FSI simulations	29
4.1	Introduction	29
4.2	A large-displacement FSI model using 2D VPM	30
4.2.1	Modelling of flow around thin and deformable geometry	30
4.2.2	Nonlinear finite element analysis using corotational beam	34
4.2.3	Presentation of immersed thin structures in the fluid domain	38
4.2.4	Calculation of the nodal forces for the structure analysis	40
4.2.5	Projection of motion from mid-surface to boundary panels	42
4.2.6	Fluid–structure coupling	43
4.2.7	Validation of the enforcement of velocity boundary condition	44
4.3	The pseudo-3D VPM for FSI simulations of flexible thin-shell structures	47
4.3.1	Multi-slice modelling of flow around deformable geometry	52
4.3.2	A linear structural model for pseudo-3D multi-slice solver	52
4.3.3	Slice-wise presentation of thin structures in fluid flow	54
4.3.4	Slice-wise fluid–structure coupling	57
4.4	A simplified aeroelectromechanical coupled model	57
4.5	Methods of inflow fluctuations for FSI simulation	59
4.6	Summary	59
5	Fluid–structure interaction simulations of thin-walled structures	61
5.1	Introduction	61
5.2	Validation of the two-dimensional coupled solver	61
5.2.1	Flexible cantilever in von Kármán vortex street	61
5.2.2	Flutter instability of cantilevered flexible plate	66
5.2.3	Aeroelastic motion of inverted flexible cantilever plate	68
5.3	Rotational flutter of inverted T-shaped cantilever with tip mass	73
5.4	Aeroelastic motion of different inverted cantilevers	74
5.5	Coupled interactions of flexible membrane systems	78
5.5.1	Flow over a building with elastic membrane roof	78
5.5.2	Aeroelastic motion of flexible 2D membrane umbrellas	84
5.6	Validation of pseudo-3D VPM for FSI simulation	92
5.6.1	Flexible cantilever in von Kármán vortex street	92
5.6.2	Identification of analytical critical flow speed of inverted flag	96
5.6.3	Flapping of skewed inverted cantilever plate	98
5.7	Vortex-induced vibration of clamped circular pipes using pseudo-3D VPM	100
5.7.1	System description and the resonance wind speed	100
5.7.2	Single-slice VIV analysis using 2D SDOF model	102
5.7.3	VIV of clamped circular pipe using pseudo-3D VPM	103
5.7.4	Ovalling response of circular pipe at higher wind speeds	106
5.8	Aeroelastic analysis of a thin-walled membrane roof	109
5.9	Pseudo-3D aeroelastic analysis of solar chimney	116

5.9.1	The solar chimney power plants	116
5.9.2	Loads on solar chimneys and stability concerns	117
5.9.3	Analyses of aeroelastic response of 1500 m solar chimneys	118
5.10	Summary	128
6	Aeroelastic energy harvesting	129
6.1	Introduction	129
6.2	Vibration energy harvesting	130
6.2.1	Background	130
6.2.2	Conversion mechanisms	130
6.3	Brief review on aeroelastic energy harvesting	132
6.3.1	Flutter/airfoil-based aeroelastic energy harvesters	132
6.3.2	Energy harvesting from vortex-induced vibration	133
6.3.3	Galloping-based energy harvesters	133
6.3.4	Harvesters based on wake galloping	134
6.4	Torsional flutter-based T-shaped energy harvesters	134
6.4.1	Torsional flutter	134
6.4.2	A reference T-shaped electromagnetic energy harvester	135
6.4.3	Identification of flutter wind speed of T-shaped harvester	135
6.5	Modelling and simulation of T-shaped electromagnetic energy harvesters	139
6.5.1	Electrical damping effects in equation of motion	140
6.5.2	Modelling of energy outputs and validation	141
6.6	Physical optimization of T-shaped energy harvesters	144
6.6.1	Influential electrical parameters	145
6.6.2	Effect of physical shape on flutter-based T-shaped harvesters	146
6.7	A framework for parametric optimisation as preliminary study	148
6.7.1	Study on electromagnetic energy harvesters	149
6.7.2	Studies on different cantilevers for preliminary assessment of piezoelectric harvesting	153
6.8	Summary	155
7	Modelling the effect of free stream fluctuations on aeroelastic interactions	157
7.1	Introduction	157
7.2	Pulsating incoming flow	158
7.2.1	Background	158
7.2.2	A New Numerical Technique in VPM for Pulsating Flow	158
7.2.3	Flow fluctuations using vorticity carrying particles	161
7.2.4	Quality assessment	163
7.2.5	Convergence of the proposed numerical scheme	165
7.2.6	The influence of flow characteristics	168
7.2.7	Influence of periodic fluctuations on T-shaped harvesters	168
7.2.8	Application of pulsating flow on flexible T-shaped harvester	174
7.2.9	Pulsating flow on flexible cantilever in Kármán vortex street	176
7.2.10	Summary	177
7.3	The flow reproduction method	178

7.3.1	Introduction	178
7.3.2	A new numerical method for reproduction of flow simulation	179
7.3.3	Validation study and efficiency of flow reproduction	184
7.3.4	Quality assessment	189
7.3.5	Wake buffeting analysis	192
7.3.6	Aeroelastic interaction of T-shaped harvester in fluctuating wind	195
7.3.7	Summary	196
8	Conclusions	199
8.1	Summary	199
8.2	Conclusions	202
8.3	Recommendations for future studies	204
	Bibliography	205
	List of publications	223
	Curriculum Vitae	225

List of Figures

1.1	The Tacoma Narrows Bridge before (left) and after the collapse (right) (picture courtesy: University of Washington Libraries, Special Collections).	1
1.2	The collapse of three tall cooling towers in Ferrybridge/England (left), the moment of collapse of one tower	2
2.1	Alan Davenport wind loading chain.	7
2.2	Flow around streamlined body (left) and bluff body (right).	9
2.3	Schematic of structural response against wind speed.	11
3.1	Schematic of the boundary element discretization for a circular cross-section. The surface vortex sheet strength	23
3.2	The simulation of flow around static bluff bodies using VPM: (a) flat plate at $Re = 10^3$, (b) flat plate at $Re = 10^4$, (c) circular cylinder at	26
3.3	Extensions on dynamic analysis models within the existing framework of in-house CFD solver based on VPM	27
4.1	A partial schematic presentation of the boundary element discretisation of a thin cantilever flexible plate of thickness h , which is flapping	31
4.2	The outlook of coupled FSI algorithm only from the 2D vortex particle method.	32
4.3	The schematic presentation of structural nodes and elements at the mid-surface of the deformed thin plate, which has been shown	35
4.4	Geometric transformation between reference and corotational configuration of a typical beam element	36
4.5	Identification of projection element for each boundary panel and the sign of surface normal vector to the element.	39
4.6	Projection of fluid pressure from the boundary panels to the structural nodes: (a) the schematic shows the projection	41
4.7	Update of the geometry based on the projection of grid points of boundary panels due to the motion at the mid-surface of the thin elements.	42
4.8	Projection of the velocity components from the nodal displacements at n_1 and n_2 to the control point p of a panel.	43
4.9	Flowchart of 2D coupled VPM for large-displacement FSI simulations.	45
4.10	Flow around an inclined flat plate in free stream flow considering static and imposed oscillation	46
4.11	Comparison of the resultant flow field U at different time in case of static and forced oscillation analyses while the numerical models used are of particular concern	48
4.12	Comparison of the velocity components U_x and U_y at different monitored locations	49

4.13	Comparison of the velocity field due to the rotational motion of flat plate in uniform flow	50
4.14	Schematic description of newly extended pseudo-3D VPM for multi-slice FSI simulation of thin-walled shell-type flexible structures	51
4.15	Identification of projection element for each boundary panel and the sign of surface normal vector corresponding to local axis of the projecting element, as shown	55
4.16	Flowchart representation of coupled numerical algorithm for pseudo-3D multi-slice simulations.	58
5.1	The interaction between the vortex shedding of rigid square section with the attached flexible cantilever plate	62
5.2	Convergence study of finite element discretisation: 1st natural vibration frequency is compared based on the number of element	64
5.3	The particle maps (left of (a-c)) and corresponding flow fields (right of (a-c)) are shown for different	64
5.4	The simulation of cantilever beam under the vortex shedding from upstream square: (a) the time history of the vertical	65
5.5	Study on the frequency of response of cantilever tip: (a) frequency spectrum of the displacement time history	65
5.6	The flutter-induced flapping of a cantilevered flexible plate: (a) the plate in conventional flag configuration under axial flow	67
5.7	The instability and post-critical vibrations of a flag-type cantilever plate in axial flow	69
5.8	Schematic configuration of a cantilever plate (length $L \times$ height H) is shown in inverted flag	70
5.9	Schematic presentation of the deflected modes for an inverted flag with the increase in incoming flow speed	70
5.10	Coupled FSI simulations of the inverted flag under axial flow	72
5.11	Visualisation of the flapping of inverted cantilever plate: (a-b) shows the particle map (left) and corresponding instantaneous	73
5.12	The comparison of the vertical tip displacement of the simulated T-shaped cantilever to identify the critical flutter wind speed.	74
5.13	Flow visualisation around moving T-shaped inverted cantilever under free stream flow	75
5.14	Schematic presentation of different inverted cantilever systems in axial flow: The effect of the tip mass and vertical tip plate	76
5.15	Comparison of maximum vertical tip displacement (left) and response frequency (right) of the specific systems under different wind speeds.	77
5.16	The fluttering modes of inverted T-shaped cantilever beam at different wind speeds: 6 m/s (left), 8 m/s (middle), and 25 m/s (right).	77
5.17	The schematic of uniform flow over a membrane roof of a building.	78
5.18	The flow around rigid building and static membrane roof deformed under 32% dead load: (a) the discretisation of surface panels	80
5.19	Coupled simulation of the membrane roof at flow velocity 13.75 m/s: (top) the vertical displacement at the centre of the roof	81

5.20	Coupled simulation of the membrane roof at 13.75 m/s: (a-b) the particle map (top) and the flow field (bottom) around	81
5.21	The effect of gravity forces on system identification: comparison of membrane displacement at centre and lowest bending frequency	82
5.22	Free vibration analyses are performed using a geometrically nonlinear finite element model of a membrane roof. Two loading scenarios are considered . . .	83
5.23	Coupled analysis of the membrane roof of a building under different flow velocities: the time history of the vertical displacement	85
5.24	A schematic presentation of two-span membrane system under uniform flow. .	86
5.25	The convecting particles in free stream flow of 10 m/s around the membrane roof.	86
5.26	Aeroelastic analysis of two-span membrane roof with a roller-type central support (a); the coupled simulations are performed	87
5.27	Aeroelastic response of two-span membrane roof with a hinged-type central support (a); the coupled simulations are performed	88
5.28	System configuration for the flow over a membrane roof.	89
5.29	Geometrically nonlinear finite element model of membrane umbrella for eigenvalue analysis: (a) the modelled system, (b) steel frame	89
5.30	Aeroelastic response of two-span membrane roof under different wind velocities: (a) 10 m/s, (b) 20 m/s, and (c) 30 m/s. For each wind speed	90
5.31	Particle maps influenced by sequential coupled motion of the membrane at 30 m/s.	91
5.32	The trajectories of nodal response for the membrane and steel frame. The red dotted lines show the original position of the structural nodes.	92
5.33	The coupled response of the membrane supports at 30 m/s: (a) left support, (b) centre support, and (c) right support.	93
5.34	The pseudo-3D VPM analysis: the interaction between a flexible cantilever beam and vortex shedding from attached rigid square cylinder	94
5.35	The schematic shows the system discretisation of the system in each simulation slice. The surface of the rigid square and flexible plate is discretised	94
5.36	The multi-slice visualisation of flexible cantilever plate in Kármán vortex street: (top) the particle maps, and (bottom) the velocity	95
5.37	The tip displacement of the cantilever plate at the mid-slice ($\xi_{z_i} = 0.5$) position (left), and the normalized frequency	96
5.38	Schematic presentation of 7-slice simulation: the flapping of inverted cantilever plate.	96
5.39	Normalized natural vibration modes and frequencies of the reference inverted cantilever plate model	97
5.40	The vortex street around the the cantilever plate at different slices due to the free stream flow.	97
5.41	The vertical tip displacement of the inverted cantilever plate at the central simulation slice ($\xi_z = 0.5$) under different dimensional	98
5.42	Schematic presentation of a skewed inverted cantilever for pseudo-3D VPM analysis: (a) the modification over the reference inverted	99
5.43	Normalized natural vibration modes and frequencies of the skewed inverted cantilever plate model	99

5.44	Pseudo-3D VPM analysis of a skewed inverted cantilever: the time histories of tip displacements	100
5.45	Vortex-induced vibration analysis of a both-end clamped circular pipe using 7-slice pseudo-3D VPM with flexible formulation:	101
5.46	The finite element modelling of the both-end clamped circular pipe and the natural vibration modes associated	102
5.47	Simulation of flow passed a static circular section: (a) the shedding of vortices behind a static circular cylinder at	103
5.48	Single-slice VIV analysis of a rigid circular section using 2D VPM with SDOF model: the normalized vertical displacement of the circular pipe	104
5.49	A 2D single-slice coupled FSI simulations of circular cylinder: (a) the peak vertical response and (b) vortex shedding frequencies at different flow velocities.	105
5.50	Pseudo-3D multi-slice simulation of a both end clamped circular pipe: the instantaneous flow fields around the circular cylinders at each slices	106
5.51	Multi-slice VIV analysis of flexible and long circular cylinder using pseudo-3D VPM with MDOF model: the normalized vertical	107
5.52	The shell buckling at the midspan of circular pipe is shown for two different phases under wind speed	108
5.53	The superposition of the surface displacements at the midspan ($\xi_z = 0.5$) of the circular pipe under the free stream wind velocities	109
5.54	Pseudo-3D multi-slice VPM model for aeroelastic coupled simulation of the flexible and long circular pipe under 45 m/s	110
5.55	Schematic configuration of a membrane roof system under free stream flow U_∞ . The roof is considered curved in a parabolic way	111
5.56	The FE model of the cantilever curved roof: (a) the thin roof is modelled by flexible membrane which is supported by a steel frame	113
5.57	Instantaneous particle map of pseudo-3D roof system under laminar flow of 30 m/s.	113
5.58	The pseudo-3D coupled simulation of the membrane roof: (a) the time histories of tip displacement at different slices of the roof under wind speed of 30 m/s .	114
5.59	The pseudo-3D coupled simulation of the membrane roof: (a) the time histories of tip displacement at different slices of the roof under wind speed of 40 m/s .	115
5.60	The free vibration analysis of the roof after the imitation of LCO at 40 m/s: (a) the time histories of tip displacement, and (b) the frequencies	116
5.61	Schematic solar chimney power plant.	117
5.62	Variants of solar chimneys of different height.	118
5.63	Details of a 1000 m solar chimney.	119
5.64	The finite element modelling of 1500 m tall solar chimneys with 3D and top views: (left) the system without any stiffening, (right) the stiffening	121
5.65	Analysis of the finite element model of 1500 m tall solar chimney (hollow configuration): the natural vibration modes and frequencies	122
5.66	Pseudo-3D aeroelastic analysis of 1500 m tall solar chimney (hollow configuration) under the wind speed of 30 m/s	123
5.67	Comparison of relative horizontal and vertical displacements at the top slice considering the monitored nodes	124

5.68	Analysis of the finite element model of 1500 m tall solar chimney (with PT tendon at regular interval): the natural vibration modes and frequencies	125
5.69	Aeroelastic response of a 1500 m tall solar chimney at wind speed of 70 m/s (stiffened SC): the time histories of horizontal	126
5.70	The aeroelastic response of 1500 m tall solar chimney under the wind speed of 70 m/s.	126
5.71	Aeroelastic analyses of 1500 m solar chimney at different wind speeds: comparison of horizontal and vertical response time histories	127
6.1	Schematic representation of the energy harvesting: (a) piezoelectric harvester, and (b) electromagnetic generator.	130
6.2	Schematic purely rotational motion of a bridge deck.	134
6.3	Electromagnetic energy harvesting from fluttering response of T-shaped cantilever systems: (a) the experimental wind tunnel set-up of a prototype T-shaped electromagnetic energy harvester	136
6.4	Modeling of T-shaped cantilever harvester: (a) the actual deformed shape of the flexible harvester	137
6.5	The flutter derivative A_2^* of the cantilever harvester obtained from forced vibration simulation	137
6.6	The use of simplified rigid beam model to identify the critical flutter wind speed based on the vertical tip displacement of the T-shaped harvester. . . .	138
6.7	The particle maps at wind speed 5 m/s in case of simplified rigid beam model.	138
6.8	Discretisation of the T-shaped cantilever harvester: (top) the discretisation scheme of the cantilever system for the flow solver and structural solver together	139
6.9	Coupled simulation of flexible T-shaped cantilever system: the flow fields around the deformed body are shown for sequential three vibration phases. . .	140
6.10	Fully coupled simulation of the T-shaped system under different wind speeds: Identification of critical onset flutter wind speed based on the aeroelastic coupled response	140
6.11	The damping of the prototype harvester: (top) total damping of the harvester estimated in reference study	142
6.12	Comparison of the time histories of the tip responses (left) and predicted voltage outputs of the harvester considering different electrical resistances . . .	143
6.13	Comparison of the energy outputs of the reference prototype T-shaped harvester under different wind speeds and electrical resistances	144
6.14	Identification of critical flutter onset load resistance (R_L) of the prototype harvester: critical R_L identified based on	145
6.15	The influence of vertical plate height H_{vp} on power output of reference T-shaped harvester: (a) the reference harvester, (b) the modified harvester . . .	146
6.16	Modification in length and thickness of the reference T-shaped harvester, and corresponding changes in dynamic properties and electrical damping ratios . .	147
6.17	Comparison of the modelled power output of the studied harvesters along with the reference harvester under the wind speed of 8 m/s and load resistance . . .	148
6.18	Comparison of influential response parameters of T-shaped cantilever with tip mass under different incoming flow	150
6.19	The average peak vertical tip displacements (a) and response frequency (b) of the T-shaped cantilever	150

6.20	The predicted power outputs of T-shaped cantilever harvester are compared in (left) and (right) for different electrical damping under U_∞ of 10 m/s and 15 m/s.	150
6.21	The electrical damping for different coupling coefficients $Nl\beta$ and load resistances R_L considering $R_C = 300 \Omega$	151
6.22	Coupled analysis of a geometrically optimized T-shaped harvester under different wind speeds	152
6.23	Schematic representation of piezoelectric energy harvesting from the vibration of cantilever beams under	153
6.24	Analysing the potential of piezoelectric energy harvesting of different cantilever systems for a wide range of wind speeds	154
6.25	Preliminary investigation on the potential of piezoelectric energy harvesting of different cantilever systems	155
7.1	The schematic of a proposed numerical scheme for the simulation of pulsating incoming flow within the framework	159
7.2	Study on the induced velocity field due to the regular seeding of the particles: (a) the discrete-time histories	162
7.3	Periodic flow fluctuations by releasing predefined vortex particles ($u_m/U_\infty = 0.15$, $fL/U_\infty = 0.1042$):	164
7.4	Quality assessment of the modelled periodic flow that has been presented . . .	166
7.5	Convergence study to validate the proposed numerical scheme by simulating a target sinusoidal flow	167
7.6	The influence of the number of particles (N_P) on the time histories of particle strength	167
7.7	The quality of the modelled flow is presented with respect to the targeted peak velocity amplitude and the frequency of flow fluctuations.	169
7.8	Dynamic motion of the harvester under steady and periodic incoming flow: comparison of the incoming field and the flow field	171
7.9	Study on the dynamic motion of the harvester under steady U_∞ and periodic incoming flow	172
7.10	Comparison of the vertical displacements of the modelled harvester under steady U_∞ and periodic incoming flow	173
7.11	The effect of the fluctuation frequency on the motion of modelled harvester: the envelopes are compared for vertical displacement under	174
7.12	The dynamic motion of the harvester under periodic flow of high fluctuations at very low frequency	175
7.13	The study on flexible T-shaped harvester under pulsating flow, which is composed of three different low frequencies	176
7.14	Study on the influence of pulsating flow on Kármán vortex street and further on coupled response of flexible cantilever: (a) schematic problem	177
7.15	Flexible cantilever response in Kármán vortex street influenced by low frequency periodic flow	178
7.16	Schematic of flow reproduction method: An upstream section ($B_1 \times D_1$) in free stream flow U_∞ , a downstream section ($B_2 \times D_2$) for wake buffeting . . .	180
7.17	Circulation around a typical square sampling-cell from the velocity sampling system	180

7.18	The reproduction simulation of flow past a square section by sequential seeding of precalculated vortex particles into the free stream flow: The comparison of .	183
7.19	Convergence study of FRM: The original flow field (a) is reproduced in four different scenarios by releasing	185
7.20	Computationally effective techniques in flow reproductions: Implementation of particle remeshing in flow reproduction	186
7.21	The influences of strength reduction factor (α_{rf}) on the quality of flow reproduction based on the comparison of characteristic flow profiles	189
7.22	The comparison of instantaneous fluctuating velocity components $u(t)$ and $w(t)$	190
7.23	Spectrum of time history of fluctuating velocity components $u(t)$ (left) and $w(t)$ (right) from the signals shown in Fig. 7.22.	190
7.24	Reproduction of simulations of different flow phenomena	191
7.25	The reproduced flow quality influenced by the location of the velocity sampling system or the particle release location (l_r) based on characteristic flow profiles	191
7.26	The effect of computationally effective techniques on the quality of flow reproduction based on the comparison	192
7.27	Normalized spectrum of the lift coefficient time history: the upstream square section in the original simulation at Reynolds number $Re = 500$	193
7.28	Dynamic simulations of the downstream section under different inflow conditions	194
7.29	Fluctuating velocity components of reproduced wakes from upstream bodies: (left) velocity time history, and (right) frequency spectrum.	195
7.30	Coupled simulation of flexible harvester in the reproduced wakes: (a) instantaneous particle map and flow field around	196
7.31	Fluctuating velocity components of random free-stream turbulence: (left) velocity time history, and (right) frequency spectrum.	197
7.32	Coupled simulation of flexible harvester in the free-stream random turbulent flow: (a) instantaneous particle map and flow field around	197

List of Tables

1.1	The FSI models are summarized based on the combination of coupling between fluid and structural solver and the incoming flow conditions.	6
4.1	Numerical parameters: the forced oscillation of an inclined flat plate.	46
5.1	Benchmark FSI problem of aeroelastic motion of an elastic cantilever attached to a square bluff body	62
5.2	Benchmark FSI problem of aeroelastic motion of an elastic cantilever attached to a square bluff body: numerical parameters	63
5.3	Comparison of current results with those in the open literature for the elastic flexible cantilever	66
5.4	Physical parameters of a cantilevered flexible plate in axial flow (mass ratio $\mu = 0.5$).	67
5.5	The flapping of cantilever plate in conventional flag configuration: numerical parameters for 2D coupled VPM analysis.	68
5.6	The physical parameters of the reference inverted cantilever plate	71
5.7	The analysis of flapping of an inverted cantilever plate in axial flow: numerical parameters for 2D coupled VPM analysis.	71
5.8	Flow over a building with elastic membrane roof: the dimensions and physical properties of fluid and membrane.	78
5.9	Flow over a building with elastic membrane roof: numerical parameters for 2D coupled VPM analysis.	79
5.10	Physical properties for the fluid and solid (membrane) two-span membrane system.	86
5.11	The numerical parameters of fluid and structural solvers for aeroelastic coupled simulation of two-span membrane system.	86
5.12	Flexible cantilever plate in Kármán vortex street: physical and material properties of the fluid and flexible plate.	94
5.13	Flexible cantilever plate in Kármán vortex street: numerical parameters for pseudo-3D coupled VPM analysis.	95
5.14	The flapping of an inverted cantilever plate in axial flow: numerical parameters for pseudo-3D VPM analysis.	97
5.15	The VIV analysis of both-end clamped thin circular pipe: the dimensions of the problem and physical properties for solid and fluid.	101
5.16	Vortex-induced vibration of clamped circular pipe: numerical parameters for pseudo-3D coupled VPM analysis.	105
5.17	The physical properties and considered dimensions for the cantilever roof system.	112
5.18	Aeroelastic response analysis of a membrane roof: numerical parameters for pseudo-3D coupled VPM analysis.	112

5.19	The physical dimensions of 1500 m solar chimney	120
5.20	Numerical parameters for aeroelastic response analyses of 1500 m tall solar chimneys.	122
6.1	Physical dimensions and dynamic properties of the reference prototype T-shaped electromagnetic energy harvester.	135
6.2	Fully coupled simulation of the T-shaped cantilever harvester: numerical parameters.	139
7.1	Simulation to induce additional constant velocity component to the free stream flow: numerical parameters.	162
7.2	Study on the harvester motion depending on the mean flow and the fluctuation amplitude: numerical parameters.	170
7.3	Study on the harvester motion depending on the mean flow and the fluctuation amplitude: numerical parameters.	175
7.4	Physical properties for the fluid and solid domains of the benchmark	182
7.5	Convergence study: numerical parameters associated with reproduction simulations performed by seeding different number of particles.	184
7.6	Adaptive numerical techniques in FRM: Numerical parameters associated with reproduction simulations.	187
7.7	Run-time comparison of simulations using different FRM techniques. Here, NP represents the average number of particles in simulation domain	188
7.8	Comparison of Run-time of the wake buffeting simulations using different computationally effective techniques in FRM.	194

Nomenclature

Greek Letters

α	Section rotation
α_{rf}	Strength reduction factor
β	Magnetic flux density
\mathcal{K}	Velocity kernel
ω	Vorticity
Φ	Mode shape matrix
Φ_{num}	Number of vibration modes
$\Delta s_{(slice)}$	Panel length in a flow analysis slice
Δt_{orig}	Original simulation time step
Δt_{rep}	Reproduction simulation time step
γ_0	Surface vorticity sheet strength
Γ_a	Approximated particle strength
Γ_m	Modified strength of vortex particle
κ	Non-dimensional flow velocity
λ	Wavelength of the periodic flow
μ	Mass ratio
ν	Poisson ratio
ν_f	Kinematic viscosity
Ω	Angular velocity
Ω_F	Fluid domain
Ω_S	Structure domain
ρ_f	Density of fluid
ρ_s	Density of solid
σ	Standard deviation

θ	Wind angle of attack
Θ	Electromechanical coupling coefficient of piezoelectric beam
ξ_{z_i}	Non-dimensional position of a flow simulation slice
ζ	Structural damping ratio
ζ_e	Electrical damping ratio
Δs	Panel length
Δt	Time step
Δt_f	Time step of flow solver
Δt_f^*	Non-dimensional time step of flow solver
Δt_r	Particle release time step
Δt_s	Time step of structure solver
Δt_s^*	Non-dimensional time step of structure solver
Γ_p	Vortex strength

Latin Letters

\mathbf{n}	Surface unit normal vector
$corr$	Correlation coefficient
cov	Covariance
h	Thickness of a plate
\mathbf{b}	Right hand side vector
$\ddot{\mathbf{d}}$	Vector of nodal acceleration
$\dot{\mathbf{d}}$	Vector of nodal velocity
\mathbf{d}	Vector of nodal displacement

\mathbf{f}_{ext}	VecExternal force vector	t_h	Thickness of harvester plate
\mathbf{f}_g	Global force vector	t_n	Time at n^{th} step
\mathbf{f}_l	Local force vector	u	Longitudinal fluctuating velocity
\mathbf{q}	Modal displacement vector	u_m	Peak longitudinal velocity fluctuation
\mathcal{B}	Transformation matrix	v	Velocity of nodal displacement
\mathcal{B}, Σ	Interface between fluid and solid region	w	Vertical fluctuating velocity
\mathbf{u}	Velocity	w_d	Width of the domain
\mathbf{x}_{c_i}	Control point of surface panels	X, Y, Z	Spatial coordinates
\mathbf{x}_p	Particle position	x, y, z	Spatial coordinates
$\mathbf{b}_{(t_n)}^s$	Right hand side vector for slice s at time t_n	x_{g_i}, y_{g_i}	Position of grid points
$\mathbf{b}_{(t_n)}$	Right hand side vector at time t_n	\bar{U}	Mean longitudinal velocity
\vec{e}	Element vector	\mathcal{M}	Influence matrix
\vec{p}	Panel vector	$\mathcal{M}_{(t_n)}$	Influence matrix at time t_n
d_x, d_y, α_z	Nodal displacements and rotation	$\tilde{\mathbf{P}}$	Modal force vector
d_y	Vertical displacement at a location	\mathbf{K}_t	Tangent stiffness matrix
$d_{y,t}$	Vertical tip displacement	$\mathcal{R}e$	Reynolds number
F	Total normal fluid force on panel	$\mathcal{S}c$	Scruton number
f, f_r	Response frequency	$\mathcal{S}t$	Strouhal number
F_n	Normal fluid force on panel n	\mathbf{C}	Damping matrix
f_n	Natural frequency of n^{th} vibration mode	\mathbf{K}	Stiffness matrix
f_s	Vortex shedding frequency	\mathbf{M}	Mass matrix
h_s	Distance between two seeding points	C_e	Electrical damping of harvester
l_d	Length of the domain	$C_{e(\text{crit})}$	Critical electrical damping
l_{coil}	Total length of the coil	E	Modulus of elasticity
l_{elem}	Length of beam element	H	Height of a system
n_i	Node numbers	I_u, I_w	Turbulence intensities
n_s	Number of step for sampling	L	Length of a system
p	Pressure	M	Mass of tip magnet
p_i	Velocity monitoring points	NT	Number of time steps
p_{ax}, p_{ay}	Panel accelerations	P_e	Electromagnetic power output
p_{vx}, p_{vy}	Panel velocities	P_p	Piezoelectric power output
s	Slice number	R_C	Electrical coil resistance
t	Time	R_L	Electrical load resistance
		RT	Run-time of a simulation
		U	Resultant velocity field
		U_∞	Free stream velocity
		U_x	Longitudinal flow velocity
		U_y	Vertical flow velocity

Chapter 1

Introduction

1.1 Background and motivation

Fluid–structure interaction (FSI) is a multiphysics study that focuses on the mutual dependence between deformable structure and surrounding or internal fluid flow. The flapping flag and the falling of a leaf are amongst the daily life FSI examples. FSI frequently encounters in many areas of civil, mechanical, aerospace and biomechanical engineering such as the aeroelastic phenomena in long-span bridges, tall towers, chimneys, and lightweight membrane systems, the motion of wind-turbine blades, the fluttering of aeroplane wings, the flow-induced vibration of marine risers, heat exchanger tubes, and the blood vessel dynamics, etc.

Structures under wind action can exhibit a variety of aerodynamic phenomena, which can lead to destructive and catastrophic events. Under specific wind–structure interaction (WSI) scenario, the aerodynamic forces can insert on a structure as a consequence of its motion, also known as self-excited forces, which cause aeroelastic instability. The incident that took attention of the bridge engineers worldwide is the historical Tacoma Narrows Bridge disaster (Fig. 1.1) in 1940, which was not entirely comprehended back at that time due to the lack of understanding of self-excited forces. Furthermore, three of a group of eight tall thin-walled cooling towers (375 ft high) collapsed in Ferrybridge/England in 1965 (c.f. Fig. 1.2), which



Figure 1.1: The Tacoma Narrows Bridge before (left) and after the collapse (right) (picture courtesy: University of Washington Libraries, Special Collections).

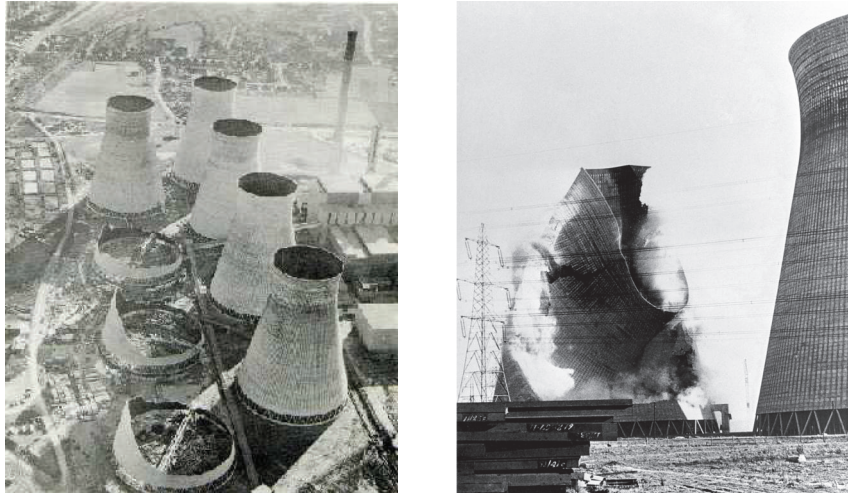


Figure 1.2: The collapse of three tall cooling towers in Ferrybridge/England (left), the moment of collapse of one tower (right) (picture courtesy: www.halinaking.co.uk).

was due to disregarding of wind action enhanced by powerful Kármán vortex street. Four towers which were on the windward side survived the wind action, but those behind were strongly affected by the vortices induced from the upstream bodies.

The design criteria of megastructures, such as long-span cable-supported bridges, super-tall buildings, towers and chimneys, large membrane roofs, are governed by the aeroelastic interaction phenomena. Advancement in computer-based numerical modelling as well as the improvement in the wind tunnel test aid to push the boundary limit of these structures. However, the desires to go beyond introduce explicit challenges for their safety and performances, mainly when they are in demand to be increasingly aesthetic and flexible. The vast majority of these structures are built in the atmospheric boundary layer, which implies that they are exposed to high turbulence flow and other effects of climate changes due to the surge of extreme events. Accurate prediction of WSI in the design process is crucial to avoid potential damage of important structures.

While the wind effects on civil engineering structures are of significant concern, the WSI has been used for large-scale wind power generation in many parts of the world. Due to the increasing demand for energy, Professor J. Schlaich of Stuttgart University proposed a solar chimney power plant (SCPP) in 1978 for solar-based electrical energy in the deserts. Conceptually, the efficiency of power generation depends largely on the chimney height and the enlargement of the heat collector area at the base. The feasibility studies on such large thin-walled chimneys proposed for different heights of 1000–1500 m and diameters of 120–170 m. Apart from several other critical design issues, such a tall vertical cantilever tower is strongly susceptible to aeroelastic buckling of thin shells. Accurate modelling and analysis of coupled behaviour have been a significant concern.

The application fields of WSI have not been limited to large-scale wind energy harvesting. In recent years, aeroelastic responses or limit cycle oscillation (LCO) of thin-plate systems have been converted to electrical energy. It has been an active research area of the last decade because of the boom in structural health monitoring, which is influenced further by the advancements in wireless sensor networks. The harvesters offer green power as an alternative to the traditional limited-life batteries, which can save maintenance costs, particularly for extensive network systems. However, the sustainable motion of aeroelastic energy harvesters is a prerequisite for energy extraction. Proper understanding of the aero-electro-mechanically

coupled interaction of thin-walled harvesters is necessary for study on energy optimisation.

It is challenging to analyse FSI problems using analytical methods since they are intrinsically nonlinear and time-dependent. Experimental studies are always considered as a standard procedure; however, the advantages that make the numerical methods increasingly widespread are their ability to predict the full-scale aerodynamic behaviour, modelling of complex shapes, and detailed visualisation of interesting flow phenomena around bluff or moving flexible bodies. They hold further some preferred components, such as low cost and easy controlling of input parameters for fluid and structural models.

The numerical methods to solve FSI problems can broadly be classified as *monolithic* and *partitioned* based on the coupling algorithm. The monolithic algorithms solve the governing equations of fluid and structural dynamics simultaneously, and therefore, they are highly robust and stable. However, monolithic algorithms are computationally costly and require substantial expertise for code preservation. In contrast, partitioned algorithms are extensively used since they allow synthesizing independent computational schemes for the fluid and the structural dynamics subsystems. However, the stability of the coupled method requires special attention. With the advancements of the computational fluid dynamics (CFD) and computational structural mechanics, significant research on FSI has been performed. However, it is still challenging to answer many of the fundamental questions in FSI concerning appropriate coupling scheme, accuracy, robustness, performance, and applicability of the simulation techniques, which indicates the need for further developments.

The Vortex Particle Method (VPM) has been established as an accurate and efficient CFD simulation technique to model flow around complex geometries. The particle-based VPM has been a viable alternative to grid-based schemes for its strength in preserving rotational flow features, which drive separation, reattachment and vortex shedding behaviour. The existing FSI implementations of VPM, which are mainly in the context of two-dimensional (2D) and pseudo-three-dimensional (pseudo-3D) formulations, have successfully been used for the analysis of aeroelastic interactions of line-like flexible structures such as long-span cable-supported bridges and towers. The existing 2D VPM can perform FSI simulation of rigid cross-sections with 3 degrees of freedom only. The pseudo-3D VPM, as the name suggests, uses multiple slices of 2D VPM simulations along the longitudinal direction of the structure to represent the full-scale 3D FSI phenomena. Even though vortex methods have successfully been used for bluff-bodies and in bridge aerodynamics; there exist no noticeable contributions in VPM for FSI analysis of deformable geometry that can be widely accepted in practical applications. The possibility of analysing flow around thin-walled flexible bodies would allow VPM to investigate a new class of FSI problems such as the flow-induced bending of a thin-plate or the deformation of thin-walled shell structures.

1.2 Objectives, methodologies and contributions

The main objective of this study is to extend the applicability of VPM for coupled FSI simulations of thin-walled flexible structures under steady and fluctuating incoming flows. The initial task is to extend the 2D VPM such that the flow-induced large motion of flexible thin bodies can be analysed. The subsequent task is to extend the pseudo-3D VPM for multi-slice FSI analysis of shell-type systems. In addition to validation of the extended FSI models, it is important to demonstrate their suitability to different FSI problems and application field of thin-walled structures. The final and compelling task is to investigate the interaction between fluid and structure influenced by inflow fluctuations.

In this context, the flow around deforming thin bodies is to be analysed using the 2D and pseudo-3D implementations of VPM. The structural behaviour is modelled and analysed using the Finite Element Method (FEM). The partitioned numerical approach is considered because of the flexibility of using different mathematical procedures for solving fluid and solid mechanics. The advantage of VPM is that the method is primarily grid-free; there is no need for conforming of mesh at the interface of fluid and structure. The structural equations are formulated and analysed at the mid-surface of the thin element because of its efficiency of handling large deformation. It is important to note that the coupled numerical extensions are based on non-conforming mesh since the interface of fluid and structure is separate. The accuracy of such models largely depends on the appropriate projection of information from one interface to another and satisfaction of the required boundary conditions.

The interest of this study includes applying the FSI models under both laminar and fluctuating incoming flows. The VPM allows including vorticity carrying particles in the free stream flow, which can create flow fluctuations in the simulation domain while convecting downstream. Prior knowledge about the characteristics of the vortex particles is necessary to achieve the desired flow fluctuations.

This thesis separates the existing FSI models of VPM from the new contributions that allow the extended coupled methods to analyse FSI of thin-walled flexible structures. The latest advancements of the VPM, the governing equations of structural analysis, and the coupling of the fluid and structural models are explained in the same chapter (Chapter 4). The validation of the coupled methods and their application are presented in the next chapters for different FSI problems. Finally, the thesis presents two further numerical extensions of VPM that allow the modelling of inflow fluctuations along with their application in FSI simulations.

The numerical extensions, the methodology, and the contribution of this research are summarized as follows:

- A partitioned algorithm of 2D VPM for large-displacement FSI simulation of thin-walled flexible systems.

It is a newly developed partitioned FSI model using 2D VPM. The model is implemented mainly for large-displacement coupled interactions of thin-plate systems. The 2D VPM with immersed interface technique is utilised for analysis of flow around deformable bodies; the method ignores cross-flow effects. The 2D corotational finite element formulation is used to analyse the geometric nonlinear motion of thin-plate systems.

- A partitioned algorithm using pseudo-3D VPM for FSI analysis of linear shell-type structures.

It is another new extension of VPM in the context of pseudo-3D multi-slice FSI analysis. Here, the structural equations are solved using superposition of uncoupled natural vibration modes, and therefore, the method is for linear structures. The novel contribution is the inclusion of 3D vibration modes of shell structures in contrast to the existing line-like structural model based on beam elements. This new extension allows simulating FSI problems of thin-walled shell structures such as large membrane roofs, tubes, towers, and chimneys, etc.

- A simplified aeroelectromechanical coupled model within the framework of 2D coupled VPM.